ACS APPLIED MATERIALS & INTERFACES

Letter

www.acsami.org

Self-Running Ga Droplets on GaAs (111)A and (111)B Surfaces

Songphol Kanjanachuchai*,† and Chanan Euaruksakul‡

†Semiconductor Device Research Laboratory (Nanotec Center of Excellence), Department of Electrical Engineering, Faculty of Engineering, Chulalongkorn University, Bangkok 10330, Thailand

‡Synchrotron Light Research Institute, 111 University Avenue, Muang District, Nakhon Ratchasima 30000, Thailand

Supporting Information

ABSTRACT: Thermal decomposition of GaAs (111)A and (111)B surfaces in ultrahigh vacuum results in self-running Ga droplets. Although Ga droplets on the (111)B surface run in one main direction, those on the (111)A surface run in multiple directions, frequently taking sharp turns and swerving around pyramidal etch pits, leaving behind mixed smooth-triangular trails as a result of simultaneous in-plane driving and out-of-plane crystallographic etching. The droplet motion is partially guided by dislocation strain fields. The results hint at the possibilities of using subsurface dislocation network and prepatterned, etched surfaces to control metallic droplet motion on single-crystal semiconductor surfaces.

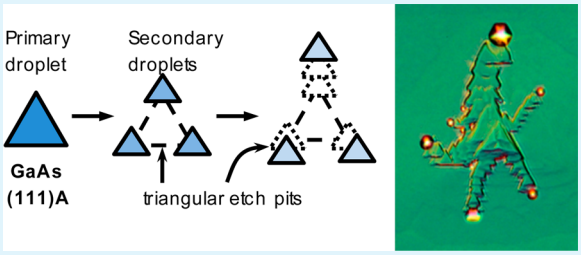

KEYWORDS: *Ga droplets, GaAs (111), self-running, stick−slip, thermal etching, mirror electron microscopy*

Metallic droplets on semiconductor surfaces are of great technological importance since they are critical to many growth/fabrication processes that employ them, for examples, as a starting material such as droplet epitaxy,[1,2] as an intermediate template such as self-catalyzed nanowires growth,[3] as a fabrication tool such as droplet drilling/etching,[4,5] or as an active layer such as plasmon-enhanced solar cells.[6] Important to most of these processes are droplets mean size, density, distribution, and control. Although positional control of droplets can, in general, be readily achieved with lithography, motion control is a relatively new design route stimulated by recent reports of self-running, or self-propelled, Ga droplets on GaAs (100)[7−9] and GaP (111)B.[10] The mechanisms driving the droplets are still controversial. On the GaAs (100) surfaces, the driving force has been attributed to chemical potentials.[7,9] But on the GaP (111)B surfaces, it has been attributed to nanoscale step elimination.[10] Few running group-III droplets has been reported to date, making it difficult to ascertain whether the two mechanisms are cation dependent, orientation specific, or even complete, thus limiting the usefulness of the self-running droplet phenomenon.

In this study, we report in situ observation of Ga droplets motion on GaAs (111)A and (111)B surfaces using mirror electron microscopy (MEM), and ex situ analyses of droplets trails using scanning electron microscopy (SEM) and Nomarski reflected light differential interference contrast (DIC) microscopy to reveal a weak, but so far neglected, droplet driving force related to dislocations. We also observed in real time the formation of a unique triangular trail morphology which we attribute to competitive effects between a stick−slip motion and crystallographic etching of Ga droplets. The results provide important insights into droplet driving mechanism, which may add another degree of freedom to the design and implementation of the various droplets-based growth and fabrication processes.

To induce and observe the running droplets, we annealed epi-ready GaAs (111)A, (111)B and (100) substrates in Elmitec's low-energy electron microscopy (LEEM) III system at 660, 620, and 630 °C, respectively. During annealing the surface is imaged in the MEM mode and video recorded. After recording their dynamics, the droplets are confirmed in situ to be metallic and ex situ to be almost pure Ga (see the Supporting Information).

Images a and b in Figure 1 show the Nomarski images of postannealed GaAs (111)A and (111)B surfaces, respectively. The GaAs (111)B, hereafter the B, surface is populated by evenly distributed droplets, in contrast to the GaAs (111)A, hereafter the A, surface which is dominated by pyramidal features with point (flat) bottoms exemplified by the structure marked with arrow a_1 (a_2), and sparsely populated by a few droplets—one of which is marked with arrow a_3. Close-up views of the A and B surfaces in images c and d in Figure 1, respectively, show droplets with triangular trail on the A and smooth trail on the B surface. Many Ga droplets on the A surface leave behind trails with mixed triangular and smooth segments. In contrast, all Ga droplets on the B surface leave behind smooth trails nearly parallel to the [01−1] direction, while those on the controlled GaAs (100) surface in Figure 1e leave behind even smoother trails along the [011] direction. Even with 10 °C lower in substrate temperature T, Ga droplets on GaAs (111)B run faster than those on GaAs (100). This is

Received: June 25, 2013
Accepted: August 13, 2013
Published: August 13, 2013

dx.doi.org/10.1021/am402455u | ACS Appl. Mater. Interfaces 2013, 5, 7709−7713

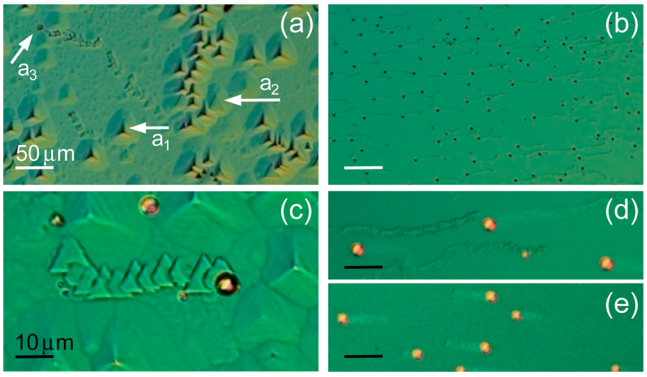

Figure 1. Nomarski DIC images showing Ga droplets and trails on GaAs (a, c) (111)A, (b, d) (111)B, and (e) (100) surfaces. The arrows in a point to (a_1) a point-bottom pyramid, (a_2) a flat-bottom pyramid, and (a_3) a Ga droplet. White (black) scale bars are 50 μm (10 μm).

due to the GaAs (111)B surface has a lower congruent temperature T_C than the GaAs (100) surface.[11] The velocity of Ga droplets on GaAs (100) has been shown[7] to vary with $(T - T_C)^2$ which qualitatively explain our results, indicating that the driving forces for Ga droplets on the GaAs (100) and (111)B surfaces are similar in nature, i.e., derive from chemical potentials.[7] Group III running droplets have only been reported in one other system—In on InAs (111)B—with little details.[12] The rest of the letter is focused on running Ga droplets on GaAs (111)A which are unprecedented and yield rich and unique information. The following features will be discussed in sequence: the background pyramidal features, preferential direction of sliding droplets, the triangular trail and the stick−slip motion.

The inverted pyramids with rounded triangular bases and point/flat bottoms dominate the background of the A but not the B surface. Similar pyramidal features on (111) surfaces have been reported in many zincblende semiconductors subject to chemical etching[13] or, as is the case here, thermal etching.[14] Their origin is attributed to edge dislocations, and their shape is bounded by the slow etching (111) plane along the ⟨110⟩ slip direction.[15,16] Their dominance on the A and absence on the B surface is not unexpected since A and B surfaces are chemically inequivalence and differ widely in many aspects, including etching behaviors.[17] Several chemical etchants reveal etch pits on the A but not the B surfaces due to selective etching of α dislocation.[17] Chemical etchings have long been used to reveal edge and to delineate line dislocations, and thermal etchings can be employed to similar effects.[18]

The background pyramidal features in Figure 1a reveal the random distribution of edge dislocations terminating at the surface. But some areas show pyramidal chains—linearly aligned pyramids—which indicate that thermal etching can also delineate dislocation lines. Images a and b in Figure 2 are Nomarski images captured from different areas of the A surface without substrate rotation. Figure 2a shows a pyramid chain along the [01−1] direction, whereas Figure 2b shows two chains along the [−101] direction. Both directions belong to one of the three dislocation axes in zincblende materials: ⟨110⟩; the other two are ⟨112⟩ and ⟨100⟩.[13] The upper chain in Figure 2b is intermittent whereas the lower chain is continuous. This possibly results from the line dislocation associated with the upper chain is further away from the surface than those associated with the lower chain. In epitaxy, subsurface dislocations can influence adatoms through surface strain fields

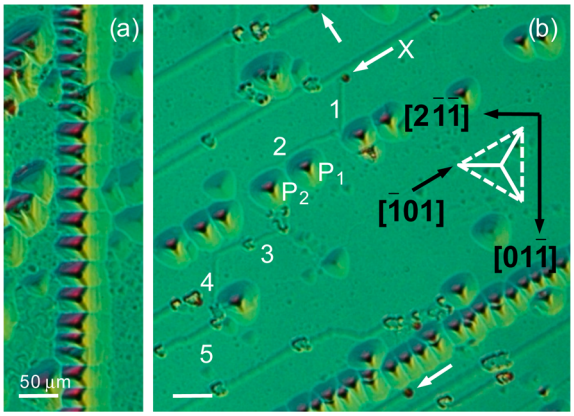

Figure 2. Nomarski DIC images showing (a) a pyramidal chain along the [01−1] direction, and (b) two pyramidal chains along the [−101] direction, droplets (white arrows), and droplet etching trails. The droplet X moves in straight lines or curves around the bases of pyramids P_1 and P_2; its etching trail is labeled 1−5 in reverse chronological order. The dotted triangle shows the (111)-bounded planes which intersect the (111) surface along the ⟨110⟩ direction. The scale bars are 50 μm.

whose magnitudes vary approximately with $1/h^2$, where h is the depth of the buried dislocation from the surface.[19] Because dislocation lines closer to the surface exert stronger forces on surface atoms, more Ga linger over them and they are thus preferentially etched, resulting in continuous pyramid chains. These chains act as Ga sinks, limiting the availability of etching material. Nearby line dislocations with comparable or weaker surface strain fields may thus be partially etched, or even unetched, leaving the fields to influence droplets motion.

An example droplet whose motion is guided by unetched dislocations is marked X in Figure 2b. Its path can be traced from its current location by the etching trail which shows 5 distinct segments with inverse chronological labels: (1) Smooth segment going in the [0−11] direction just before the droplet makes a sharp 120° turn toward its current location along the [−101] direction. (2) Smooth segment nearly parallel to the [−101] direction, indicating that the droplet has swerved around the bases of pyramids P_1 and P_2. (3) A mixed segment with triangular etched pits at the center surrounded by smooth trails. (4) Smooth segment along the [0−11] direction, i.e., parallel with segment 1. (5) A mixed segment similar to and approximately parallel with segment 3. Existing explanations of droplet driving forces due to chemical effects[7,9] or nanoscale step ordering[10] are surface/interfacial in nature, predicting straight or near straight path with deviation in the same order as substrate miscut (a few degrees) and thus cannot explain the sharp turns observed. Wu et al recently reported "daughter" Ga droplets that move orthogonally to the "mother" droplet on GaAs (100) surface and explained the observation in terms of surface roughness and chemical potential difference,[20] which cannot explain the multiple 120° turns on the GaAs (111)A surface we observed. On the contrary, our explanations below can readily explain the origin of the orthogonal droplet motions on the GaAs (100) surface observed by Wu et al.

The paths of the droplet X and nearby droplets are confined to only a few directions, all of which are parallel with the pyramids chains, strongly indicating that both structures share the same origin. Because pyramid chains delineate line dislocations, the observed droplet motion must be, at least partially, guided by the buried dislocations by virtue of surface

strain fields. The effects that subsurface dislocations have on surface adatoms are known to exist in epitaxy: dislocation networks have been used to guide the nucleation of quantum dots.[21−23] Our results demonstrate the equivalent effects on evaporating surfaces.

The effects of dislocations guiding droplet motion above is observed only at the early stages of thermal decomposition. Prolonged or overannealing will result in planarization of the trails and the population of droplets of other origins whose paths are dictated by other factors. Figure 3 shows SEM images of one type of such droplets formed from flat-bottom pyramids, a dominant feature on overannealed GaAs (111)A surfaces. Postannealed morphological analyses using Nomarski imaging and SEM show that flat-bottom pyramids are either emptied, partially- or completely filled with Ga. From the many flat-bottom pyramids at various stages, we can conclude that each pyramid is originally filled with a relatively flat, triangular Ga droplet which we refer to as the primary droplet. As heating continues, more Ga is added to the droplet, the surface area increases and the primary droplet becomes unstable. To reduce the surface area, the primary droplet is broken up into three secondary droplets, with approximately the same volume for the particular case of Figure 3a. The evolution is schematically drawn in Figure 3c. One or more of the secondary droplets are then driven out: from the smooth center of the triangular etch pit toward the roughened surroundings. The SEM image in Figure 3b (different position from Figure 3a) shows that the smallest (left) droplet has moved only "one triangle" or 1Δ away from the primary site, whereas the top droplet has moved 2Δs and the biggest (right) droplet 4Δs. The difference in droplet mobility is due mainly to size. Droplet driving force has been shown to vary linearly with droplet diameter.[7,9] Under similar surroundings, the bigger the droplet, the greater the distance, from the primary site, which qualitatively explains our results. From the trails, it can be seen that the three droplets are pushed up the flat-bottom pyramids, with faceted steps and boundaries, indicating simultaneous in-plane (forward) motion and out-of-plane (downward) etching.

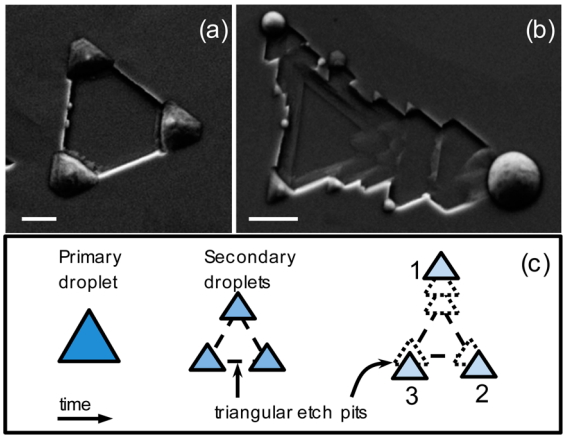

Figure 3. Nucleation and initial motion of Ga droplets formed from flat-bottom pyramids. SEM images of the pyramid and droplets (a) just after the primary droplet breaks up and form three secondary droplets at the corners, (b) after secondary droplets have vacated the primary pit. (c) Schematic drawing showing the time evolution of Ga droplet nucleation, from the primary droplet to the release of the secondary droplets from the primary etch pit. The scale bars in a and b are 5 μm.

Once droplets vacate the primary etch pit, they move in a stick−slip manner with directions dictated by the pits and the immediate surroundings. These droplets preferentially move along the corners (e.g., droplet 1 in Figure 3c), the sides (droplet 2), or the side normals (droplet 3) of the just vacated pits. The stick−slip motion of many running droplets is followed live in MEM mode where Ga droplets can be identified by dark regions surrounded by bright caustic rings.[24] Snapshots of the MEM video (see the Supporting Information) covering two complete stick−slip cycles are shown in Figures 4a−e. The droplet in this case moves along a side normal of the etched pits. The shape of the droplet in Figure 4a, c, and e can be described as rounded triangular, whereas those of images b and d in Figure 4 can be described as circular, reflecting a spherical cap shape. The rounded triangular shape forms slowly

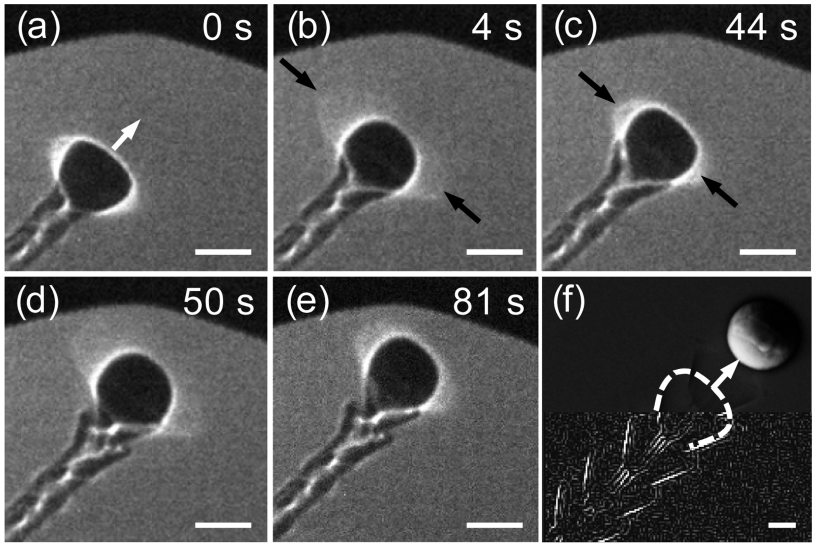

Figure 4. (a−e) Snapshots from the MEM video (see the Supporting Information) showing a Ga droplet making two stick−slip cycles. The droplet appears as a dark region surrounded by bright caustic features (black arrows in b and c). (f) SEM image of a droplet with faceted trail (lower half digitally enhanced to hi-light the edges). White dash superimposed on the trail in f is the perimeter of the droplet in a. The scale bars are 2 μm.

and is the final shape just before the droplet slips. On the contrary, the circular shape forms quickly and is the starting shape right after the droplet stops slipping, or starts sticking. At 660 °C, slipping takes a few seconds and sticking takes approximately 30−40 s. While sticking, the droplet volume slowly increases and the circular shape is distorted, finally transformed into a rounded triangle just before slipping. The perimeter of the rounded triangular droplet, observed in situ by MEM, in Figure 4a is superimposed onto the running trail of a different but similar droplet, observed ex situ by SEM, in Figure 4f. The droplet in Figure 4f is more than double the size of those in Figure 4a, yet the perimeter of the latter matches the trail of the former almost exactly. The droplet perimeter is bounded by the slow etching (111) planes. Upon etching and incorporation of Ga from the liquid/solid (droplet/substrate) interface, the droplet volume must expand by increasing height and surface curvature, triggering the droplet to spring back into the spherical cap shape. The shape of the Ga droplets on the GaAs (111)A surface thus cycles between circular and triangular. This is similar to the nonrunning Ga droplets on GaAs (100) and In droplets on InP (100), which cycle between circular and rectangular.[25,26] After attaining the spherical cap shape, the droplets always move toward the pristine surface.

The initial force driving the droplets out of the etch pits simply originate from the force imbalances right after the droplets transform from a triangular to a circular shape. The schematic cross-sections in images a and b in Figure 5 show the

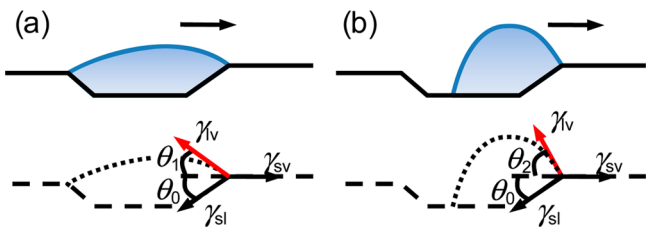

Figure 5. Schematic cross-section (upper panel) and interfacial energies (lower) at the triphase junction of the advancing front of a droplet right (a) before and (b) after its shape transforms from a triangle to a circle. The "shape" refers to the bird's-eye view.

interfacial energies at the triphase junction at the advancing front of a hypothetical droplet just before and after the shape transformation, respectively. γ_{sl}, γ_{sv}, and γ_{lv} are the solid−liquid, solid−vapor, and liquid−vapor energies, respectively. As a result of the shape transformation, the contact angle (relative to the flat planar front) increases from θ_1 to θ_2. Though no quantitative measurements are made, the contact angle change can be implied from the change of the caustic features:[24] the caustic span, the width confined by the arrows, reduces from image b to c in Figure 4 as the droplet expands in volume. Because the droplet is immobile just before the shape transformation, the horizontal energies must be balanced; i.e., $\gamma_{sv} = \gamma_{sl}\cos\theta_0 + \gamma_{lv}\cos\theta_1$. The balance is however disturbed right after the transformation because $\theta_2 > \theta_1$, resulting in a net forward force proportional to the energetic difference $\gamma_{lv}(\cos\theta_1 - \cos\theta_2)$. This force is responsible for pushing the droplet up the etch pit. If the force is sufficiently strong, the whole droplet will be pushed up and released from the pit, sliding forward and leaving a smooth trail; otherwise the droplet will cling on to the triphase junction and immediately begins etching, gaining more mass and begins the next period of the shape cycle, resulting in crystallographic steps/boundaries.

In summary, mobile Ga droplets on thermally annealed GaAs (111)A and (111)B surfaces are reported for the first time. Ga droplets on GaAs (111)B run in a manner consistent with surface forces due to chemical gradient similar to those on GaAs (100). However, Ga droplets on GaAs (111)A run in specific directions dictated by i) subsurface dislocation network for sliding droplets or ii) crystallographic etching for sticking droplets. Droplet shape transformation is found to provide a sufficient force to release/nudge sticking droplets from thermal etch pits. These insights may ultimately lead to metallic droplet motion control via dislocation networks and prepatterned, etched single-crystal surfaces.

■ ASSOCIATED CONTENT

Supporting Information

Sample preparation, Ga droplet confirmation, and running Ga droplet video. This material is available free of charge via the Internet at http://pubs.acs.org.

■ AUTHOR INFORMATION

Corresponding Author

*E-mail: songphol.k@chula.ac.th (S.K.).

Notes

The authors declare no competing financial interest.

■ ACKNOWLEDGMENTS

We acknowledge W. Busayaporn, T. Chokamnuai, C. Himwas, N. Jearanaikoon, P. Photongkam, and P. Rattanadon for assistance during MEM imaging. S.K. acknowledges Prof. S. Panyakeow for continuous supports, and grants from the Ratchadaphiseksomphot Endowment Fund of Chulalongkorn University (RES560530147-EN).

■ REFERENCES

(1) Sanguinetti, S.; Koguchi, N.; Mano, T.; Kuroda, T. *J. Nanoelectron. Optoelectron.* **2011**, *6*, 34−50.
(2) Kumah, D. P.; Shusterman, S.; Paltiel, Y.; Yacoby, Y.; Clarke, R. *Nat. Nanotechnol.* **2009**, *4*, 835−838.
(3) Fontcuberta i Morral, A.; Colombo, C.; Abstreiter, G.; Arbiol, J.; Morante, J. R. *Appl. Phys. Lett.* **2008**, *92*, 063112.
(4) Wang, Z. M.; Liang, B. L.; Sablon, K. A.; Salamo, G. J. *Appl. Phys. Lett.* **2007**, *90*, 113120.
(5) Heyn, Ch. *Phys. Rev. B* **2011**, *83*, 165302.
(6) Pillai, S.; Catchpole, K. R.; Trupke, T.; Green, M. A. *J. Appl. Phys.* **2007**, *101*, 093105.
(7) Tersoff, J.; Jesson, D. E.; Tang, W. X. *Science* **2009**, *324*, 236−238.
(8) Wu, J.; Wang, Zh. M.; Li, A. Z.; Benamara, M.; Li, S.; Salamo, G. J. *PLoS ONE* **2011**, *6*, e20765.
(9) Wu, J.; Wang, Zh. M.; Li, A. Z.; Benamara, M.; Lee, J.; Koukourinkova, S. D.; Kim, E. S.; Salamo, G. J. *J. Appl. Phys.* **2012**, *112*, 043523.
(10) Hilner, E.; Zakharov, A. A.; Schulte, K.; Kratzer, P.; Andersen, J. N.; Lundgren, E.; Mikkelsen, A. *Nano Lett.* **2009**, *9*, 2710−2714.
(11) Goldstein, B.; Szostak, D. J.; Ban, V. S. *Surf. Sci.* **1976**, *57*, 733−740.
(12) Mandl, B.; Stangl, J.; Hilner, E.; Zakharov, A. A.; Hillerich, K.; Dey, A. W.; Samuelson, L.; Bauer, G. n.; Deppert, K.; Mikkelsen, A. *Nano Lett.* **2010**, *10*, 4443−4449.
(13) Abrahams, M. S.; Buiocchi, C. J. *J. Appl. Phys.* **1965**, *36*, 2855−2863.
(14) Zeng, D.; Jie, W.; Wang, T.; Zhang, J.; Zha, G. *Thin Solid Films* **2009**, *517*, 2896−2899.
(15) Abrahams, M. S. *J. Appl. Phys.* **1964**, *35*, 3626−3627.

(16) Stirland, D. J.; Straughan, B. W. *Thin Solid Films* **1976**, *31*, 139−170.
(17) Gatos, H. C.; Lavine, M. C. *J. Electrochem. Soc.* **1960**, *107*, 427−433.
(18) Dubowski, J. J.; Wróbel, J. M.; Mitchell, D. F.; Sproule, G. I. *J. Cryst. Growth* **1989**, *94*, 41−45.
(19) Andrews, A. M.; Speck, J. S.; Romanov, A. E.; Bobeth, M.; Pompe, W. *J. Appl. Phys.* **2002**, *91*, 1933−1943.
(20) Wu, J.; Wang, Zh. M.; Li, A. Z.; Benamara, M.; Salamo, G. J. *ACS Appl. Mater. Interfaces* **2011**, *3*, 1817−1820.
(21) Shiryaev, S. Y.; Jensen, F.; Hansen, J. L.; Petersen, J. W.; Larsen, A. N. *Phys. Rev. Lett.* **1997**, *78*, 503−506.
(22) Xie, Y. H.; Samavedam, S. B.; Bulsara, M.; Langdo, T. A.; Fitzgerald, E. A. *Appl. Phys. Lett.* **1997**, *71*, 3567−3568.
(23) Kanjanachuchai, S.; Maitreeboriraks, M.; Thet, C. C.; Limwongse, T.; Panyakeow, S. *Microelectron. Eng.* **2009**, *86*, 844−849.
(24) Kennedy, S. M.; Zheng, C. X.; Tang, W. X.; Paganin, D. M.; Jesson, D. E. *Ultramicroscopy* **2011**, *111*, 356−363.
(25) Lowes, T. D.; Zinke-Allmang, M. *Phys. Rev. B* **1994**, *49*, 16678−16683.
(26) Shorlin, K.; Zinke-Allmang, M. *Surf. Sci.* **2007**, *601*, 2438−2444.